HHS Public Access

Author manuscript

Cancer Immunol Res. Author manuscript; available in PMC 2018 September 01.

Published in final edited form as:

Cancer Immunol Res. 2017 September ; 5(9): 767–777. doi:10.1158/2326-6066.CIR-16-0365.

The Tumor Microenvironment Regulates Sensitivity of Murine Lung Tumors to PD-1/PD-L1 Antibody Blockade

Howard Y. Li[1,2,*], **Maria McSharry**[2], **Bonnie Bullock**[2], **Teresa T. Nguyen**[2], **Jeff Kwak**[2], **Joanna M. Poczobutt**[2], **Trisha R. Sippel**[2], **Lynn E. Heasley**[3], **Mary C. Weiser-Evans**[2], **Eric T. Clambey**[4], and **Raphael A. Nemenoff**[2]

[1]Department of Medicine, Veterans Affairs Medical Center, Denver, CO 80220

[2]Department of Medicine, University of Colorado Anschutz Medical Campus, Aurora, CO 80045

[3]Department of Dental Medicine, University of Colorado Anschutz Medical Campus, Aurora, CO 80045

[4]Department of Anesthesiology, University of Colorado Anschutz Medical Campus, Aurora, CO 80045

Abstract

Immune checkpoint inhibitors targeting the interaction between programmed cell death-1 (PD-1) and its ligand PD-L1 induce tumor regression in a subset of non-small cell lung cancer patients. However, clinical response rates are less than 25%. Evaluation of combinations of immunotherapy with existing therapies requires appropriate pre-clinical animal models. In this study, murine lung cancer cells (CMT167 and LLC) were implanted either orthotopically in the lung or subcutaneously in syngeneic mice, and response to anti-PD-1/PD-L1 therapy was determined. Anti-PD-1/PD-L1 therapy inhibited CMT167 orthotopic lung tumors by 95%The same treatments inhibited CMT167 subcutaneous tumors by only 30%, and LLC orthotopic lung tumors by 35%. CMT167 subcutaneous tumors had more $Foxp3^+$ $CD4^+$ T cells and fewer PD-1^+ $CD4^+$ T cells compared to CMT167 orthotopic tumors. Flow cytometric analysis also demonstrated increased abundance of PD-$L1^{high}$ cells in the tumor microenvironment in CMT167 tumor-bearing lungs compared to CMT167 subcutaneous tumors or LLC tumor-bearing lungs. Silencing PD-L1 expression in CMT167 cells resulted in smaller orthotopic tumors that remained sensitive to anti-PD-L1 therapy, whereas implantation of CMT167 cells into PD-$L1^-$ mice blocked orthotopic tumor growth, indicating a role for PD-L1 in both the cancer cell and the microenvironment. These findings indicate that the response of cancer cells to immunotherapy will be determined by both intrinsic properties of the cancer cells and specific interactions with the microenvironment. Experimental models that accurately recapitulate the lung tumor microenvironment are useful for evaluation of immunotherapeutic agents.

[*]Corresponding Author: Howard Y. Li, University of Colorado Anschutz Medical Campus, Department of Medicine, Division of Pulmonary Sciences and Critical Care Medicine, 12700 East 19th Ave C-272, Aurora, CO 80045; Phone 303-724-4881; Fax 303-724-6042; Howard.Li@ucdenver.edu.

Keywords

Immunotherapy; lung cancer; programmed cell death 1 (PD-1); programmed cell death ligand 1 (PD-L1); tumor microenvironment

Introduction

A breakthrough in cancer therapy is the development of immune checkpoint inhibitors. Interaction of programmed cell death-1 (PD-1) with its ligands, PD-L1 or PD-L2, regulates peripheral tolerance and protects tissues from autoimmune attack (1). However, induction of PD-L1 expression on tumor cells can inhibit cytotoxic T cells, which allows tumors to progress (2). Evidence that PD-L1 is up-regulated in non-small cell lung cancer (NSCLC) has led to the development of immune-based therapies for NSCLC. However, response rates in NSCLC patients across clinical trials of PD-1 and PD-L1 antibodies have ranged from 14.5% to 20% (3–7). The combination of immunotherapy with existing therapies such as radiation therapy, chemotherapy, or other immunotherapeutic agents may improve response rates. Testing of such combinations and development of patient selection criteria for immunotherapy require preclinical models that mimic the human disease.

In vivo growth of lung cancer cells has been assessed by implanting human cells into immune compromised mice (xenograft models). However, these mice lack T lymphocytes, rendering this model unsuitable for examining immunotherapy. To study the role of adaptive immunity in tumor progression, implantation of murine cancer cells into syngeneic mice is required. There are few established murine lung cancer cell lines derived from C57BL/6 mice. Many studies use a subcutaneous model whereby tumors develop in the flank, which fails to reflect the lung tumor microenvironment (TME). To examine the role of the TME in lung cancer, our laboratory utilizes an orthotopic model in which murine lung cancer cells are implanted into the lungs of syngeneic C57BL/6 mice (8–11). In this study, we examined the response of tumors grown in the lung or subcutaneously to PD-1/PD-L1 inhibition. We found that sensitivity to PD-1/PD-L1 antibodies was dependent on both the site of tumor growth and the cancer cell line, and was associated with up-regulation of PD-L1 in both cancer cells and stromal cells. This study suggests that the response of lung cancer to PD-1/PD-L1 inhibition will be determined by interactions between cancer cells and non-cancer cells specific to the lung.

Materials and Methods

Cell lines

CMT167 cells (12) were stably transfected with firefly luciferase as previously described (11). Lewis Lung Carcinoma Cells (LL/2) were purchased from ATCC and luciferase-expressing Lewis Lung Carcinoma cells (LLC) were purchased from Caliper Life Sciences (LL/2-luc-M38). All cell lines were periodically tested for mycoplasma infection and were last retested in February 2017. To avoid cross-contamination and phenotypic changes, cells were maintained as frozen stocks and cultured for only two to four weeks before use in experiments. Authentication of cell lines based on morphology, growth curve analysis, and

metastatic phenotype was performed regularly, and no phenotypic changes were observed through the duration of the study.

Kras sequence analysis

Total RNA was extracted from CMT167, LLC, and LL/2 cells using an RNeasy Mini Plus Kit (QIAGEN). Reverse transcription was performed using an iScript cDNA Synthesis Kit (Bio-Rad). Kras was amplified by PCR with the following primers: For, 5′-GCCTGCTGAAAATGACTGAG-3′; Rev, 5′-TGCTGAGGTCTCAATGAACG-3′. PCR products were purified using a QIAquick PCR Purification Kit (QIAGEN) and sequenced using the reverse primer 5′-TCCAAGAGACAGGTTTCTCCA-3′.

Animals and tumor models

Wild type C57BL/6 mice and green fluorescent protein (GFP)-expressing mice [C57BL/6-Tg(UBC-GFP)30Scha/J] were obtained from Jackson Laboratory (Bar Harbor, ME). PD-L1 knockout (KO) mice on a C57BL/6 background were provided by Dr. Haidong Dong (Mayo Clinic, Rochester, MN). Animals were bred and maintained in the Center for Comparative Medicine at the University of Colorado Anschutz Medical Campus. Experiments were performed on 8–12 week old male mice. All procedures were performed under protocols approved by the Institutional Animal Care and Use Committees at the University of Colorado and Denver VA Medical Center.

Surgeries were performed under inhaled isoflurane anesthesia, and all efforts were made to minimize suffering. For orthotopic tumors, a transverse skin incision was made along the left lateral axillary line at the level of the xyphoid process, and subcutaneous fat was dissected away as previously described (9). CMT167 or LLC cells (10^5) were suspended in Hank's Buffered Salt Solution (HBSS) containing 1.35 mg/mL Matrigel (Corning) and injected through the chest wall into the left lung, and the incision was closed using veterinary skin adhesive. For subcutaneous tumors, the inoculation site was sterilized with ethanol, and CMT167 cells suspended in 100 μL HBSS were injected subcutaneously into the lower flank. Four weeks after CMT167 tumor implantation or three weeks after LLC tumor implantation, mice were injected intraperitoneally with D-Luciferin (PerkinElmer, 300 mg/kg) immediately before euthanasia. Primary tumor size was measured using digital calipers. Metastasis to the lungs, mediastinal lymph nodes, and liver were quantified by *ex vivo* bioluminescence using an IVIS 50 Imaging System (Xenogen) and Living Image software (PerkinElmer).

PD-1 and PD-L1 pharmacologic antibody blockade

Rat monoclonal antibody to mouse PD-1 (clone RMP1-14), rat monoclonal antibody to mouse PD-L1 (clone 10F.9G2), and isotype control antibodies (rat IgG2a clone 2A3 for anti-PD-1, rat IgG2b clone LTF-2 for anti-PD-L1) were purchased from BioXCell (Lebanon, NH). Tumor-bearing mice were injected intraperitoneally [200 μg in PBS per dose (8–10 mg/kg)] three times weekly starting one week after tumor implantation.

Immunostaining

Sections (5 μm thick) were cut from formalin fixed, paraffin embedded (FFPE) tissue blocks. Antigens were revealed by heating slides in Antigen Unmasking Solution (Vector Labs). Slides were blocked with 3% normal goat serum, then incubated overnight with anti-CD3ε antibody (Abcam). After washing with TBST, slides were incubated with AF488 conjugated IgG secondary antibody (Life Technologies). Slides were coverslipped with VECTASHIELD Mounting Medium with DAPI (Vector Labs). Tumor-infiltrating lymphocytes (TILs) were defined as lymphocytes within tumor cell nests or in direct contact with tumor cells. For comparison of CMT167 and LLC tumors, three sections from each animal were stained, and three random fields (40x) per section were quantified independently by two blinded observers (HYL and MM); the mean was used for analysis.

Flow cytometry

For orthotopic tumors, the pulmonary circulation was perfused with heparinized PBS and tumor-bearing left lungs were isolated. Flank tumors were dissected away from the subcutaneous tissue and were mechanically dissociated and digested with a mixture containing collagenase type 4 (8480 U/mL), elastase (7.5 mg/mL), and soybean trypsin inhibitor (2 mg/mL) (all from Worthington Industries) in HBSS. Red blood cell lysis was performed using RBC lysis buffer [0.15 M NH_4Cl, 0.1 mM $KHCO_3$, 0.1 mM Na_2EDTA (pH 7.2)]. Antibody panels are summarized in Supplementary Table S1. Samples were acquired at the University of Colorado Cancer Center Flow Cytometry Shared Resource using a Gallios flow cytometer (Beckman Coulter) and data were analyzed using Kaluza Software (Beckman Coulter). To determine the abundance of PD-L1^{high} cells in the TME, tumors were implanted in GFP-expressing transgenic mice, and the ratio of GFP$^+$PD-L1^{high} to GFP$^+$PD-L1^{low} cells was determined.

Recovery of lung cancer cells from tumor-bearing GFP-expressing transgenic mice

Three weeks after CMT167 tumor implantation or two weeks after LLC tumor implantation, tumor-bearing left lungs were isolated and single cell suspensions were prepared. Cell sorting was performed at the University of Colorado Cancer Center Flow Cytometry Shared Resource using an XDP-100 cell sorter (Beckman Coulter). Lung cancer cells were recovered from tumor-bearing GFP-expressing transgenic mice by sorting for GFP-negative cells, and total RNA was isolated using an RNeasy Plus kit (QIAGEN).

RNA sequencing (RNA-seq)

CMT167 cells were recovered from three pools of mice consisting of five GFP-expressing mice each, whereas LLC cells were recovered from five pools of mice consisting of four GFP-expressing mice each. Total RNA was also isolated from cells in culture at the time of injection. RNA-seq library preparation and sequencing were conducted at the University of Colorado Cancer Center Genomics and Microarray Shared Resource. RNA libraries were constructed using an Illumina TruSEQ stranded mRNA Sample Prep Kit. Sequencing was performed on an Illumina HiSEQ 2500 High Throughput Flow Cell. RNA-seq reads were processed and aligned to the UCSC Mus musculus reference genome (build mm10) using TopHat v2 (13). The aligned read files were processed by Cufflinks v2.0.2 (14), which uses

the normalized RNA-Seq fragment counts to measure the relative abundance of transcripts. The unit of measurement is Fragments Per Kilobase of exon per Million fragments mapped (FPKM).

Quantitative real-time PCR (qRT-PCR)

CMT167 cells were recovered from three pools of mice consisting of three tumor-bearing GFP-expressing mice each and LLC cells were recovered from four pools of mice consisting of two tumor-bearing GFP-expressing mice each, and total RNA was isolated using an RNeasy Plus Kit (QIAGEN). Total RNA was also isolated from cancer cells grown in culture, either in the presence or absence of IFNγ (100 ng/mL). Reverse transcription was performed using an iScript cDNA Synthesis Kit (Bio-Rad). Real-time PCR analysis was conducted in triplicate in an iCycler (Bio-Rad). Sequences of primers used were: PD-L1 (For: 5′-TGCTGCATAATCAGCTACGG-3′, Rev: 5′-GCTGGTCACATTGAGAAGCA-3′), β-actin (For: 5′-GGCTGTATTCCCCTCCATCG-3′, Rev: 5′-CCAGTTGGTAACAATGCCATGT-3′).

shRNA knockdown of PD-L1

Three shRNAs (sh67998, sh68000, sh68001) to mouse PD-L1 and a non-targeting control shRNA were obtained from the Functional Genomics Facility at the University of Colorado Cancer Center. Lentiviral particles were generated by transfecting shRNA vectors into 293T cells using Turbofect (Thermo Scientific). CMT167 cells were transduced with lentiviral particles and placed under puromycin selection. Cells were analyzed for PD-L1 mRNA expression by qRT-PCR and protein expression by flow cytometry as described above. The pool of cells with the highest degree of knockdown (CMT sh68001) was designated CMT shPD-L1 and used in orthotopic mouse experiments. CMT167 cells transduced with non-targeting control shRNA were designated CMT shCON.

$CD8^+$ T-cell immunodepletion

Rat monoclonal anti-mouse CD8 (clone 53-6.72) and rat IgG2a (clone 2A3) were purchased from BioXCell (Lebanon, NH). Mice were injected intraperitoneally [200 μg in PBS per dose (8–10 mg/kg)] twice weekly starting one day prior to tumor implantation and throughout the course of the tumor progression experiment.

Isolation of bone marrow derived macrophages (BMDMs) and treatment with cancer cell conditioned media (CM)

Bone marrow cells isolated from C57BL/6 mice were matured into macrophages using M-CSF (eBioscience, 50 ng/mL) as previously described (10). Two days after isolation, 25% control media, 25% LLC CM, or 25% CMT167 CM was added to bone marrow cells (CM were normalized to total protein). Culture media was replaced every three days. As a positive control, macrophages matured in M-CSF only were stimulated with recombinant mouse interferon-γ (Sigma, 100 ng/mL). For neutralization experiments, monoclonal antibodies against IL7 (BioXCell clone M25) and IL15 (eBioscience clone AIO.3) were added along with CM (10 μg/mL). After 10 days, total RNA was isolated from BMDMs.

Statistical analysis

Data are presented as mean ± SEM. Differences between groups were identified using Student unpaired *t* test or one-way ANOVA. Under all circumstances, $P < 0.05$ was considered significant.

Results

CMT167 cells, luciferase-expressing LLC cells, and LL/2 cells express oncogenic K-Ras

Although there are hundreds of human lung cancer cell lines, there are few murine lung cancer cell lines. In this study, we used two murine lung cancer cell lines derived from C57BL/6 mice, CMT167 and LLC cells. CMT167 cells have previously been reported to harbor an activating $Kras^{G12V}$ mutation (15). Direct DNA sequencing confirmed that CMT167 cells harbor a $Kras^{G12V}$ mutation (Supplementary Fig. S1A). The DNA sequencing chromatogram of *Kras* in luciferase-expressing LLC cells purchased from Caliper revealed a double peak in codon 12 that corresponded with a heterozygous activating $Kras^{G12C}$ mutation (Supplementary Fig. S1B). DNA sequencing of *Kras* in LL/2 cells purchased from ATCC revealed an identical heterozygous $Kras^{G12C}$ mutation (Supplementary Fig. S1C). Thus, these cell lines represent K-Ras mutant lung cancers.

Sensitivity of CMT167 orthotopic tumors to PD-1/PD-L1 inhibition

We have previously shown that murine lung cancer cells injected into the lungs of syngeneic C57BL/6 mice form a primary tumor, which subsequently metastasizes to the other lung lobes, mediastinal lymph nodes, and liver (10, 11). Since this model recapitulates many features of human lung cancer, we sought to determine whether orthotopic tumors are sensitive to anti-PD-1/PD-L1. Wild type C57BL/6 mice were treated with anti-PD-1, anti-PD-L1, or control IgG starting one week after CMT167 orthotopic tumor implantation. Treatment with either checkpoint inhibitor reduced primary tumor size by approximately 95%; 40% of mice receiving anti-PD-1 and 60% of mice receiving anti-PD-L1 had no detectable tumors (Fig. 1A). PD-1 and PD-L1 inhibition reduced the metastatic burden in the other lung lobes by 81% and 87%, respectively (Fig. 1B). Metastases were detected in some animals that had undetectable primary tumors, suggesting that primary tumors were initially present and regressed with checkpoint inhibitor treatment. Immunofluorescence staining of tumor-bearing lungs for CD3ε (Fig. 1C) revealed dense nests of tumor-infiltrating T lymphocytes in mice treated with anti-PD-1 [Fig. 1C(c) and 1C(d)] and anti-PD-L1 [Fig. 1C(g) and 1C(h)]. Although lymphocytes were identified in tumors from control animals [Fig. 1C(a), 1C(b), 1C(e), 1C(f)], large nests of lymphocytes were not observed. These data suggest that in our orthotopicmodel, treatment with anti-PD-1/PD-L1 leads to accumulation of TILs that mediate antitumor responses.

PD-L1 expression in CMT167 orthotopic tumors

Next, we examined *in vivo* expression of PD-L1 in CMT167 orthotopic tumors. To distinguish cancer cells from normal mouse lung epithelial cells, CMT167 cells were implanted into GFP-expressing transgenic mice. Two weeks after tumor implantation, tumor-bearing lungs were analyzed by flow cytometry. Uninjected mice were used for

controls (Fig. 2A). In mice with CMT167 orthotopic tumors, a subset of both cancer cells (GFP^-) and non-cancer cells (GFP^+) expressed PD-L1 (Fig. 2B). PD-$L1^{high}$ cells were more abundant in the microenvironment of CMT167 tumor-bearing mice than in control mice. Although cancer cells expressing high levels of PD-L1 (GFP^-;PD-$L1^{high}$) were detected, this population appeared smaller and expressed less PD-L1 than host-derived PD-$L1^{high}$ cells in the TME. To confirm PD-L1 expression on cancer cells, CMT167 cells were recovered from tumors using flow cytometry (Supplementary Fig. S2), and were compared with cancer cells grown in culture using RNA-seq. From this analysis, we determined that PD-L1 mRNA expression was induced in CMT167 cells *in vivo* (Fig. 2C). We confirmed these data in separate isolations of CMT167 cells recovered from GFP mice using qRT-PCR (Fig. 2D). As a positive control, CMT167 cells were treated *in vitro* with IFNγ to stimulate PD-L1 expression.

We have previously characterized subpopulations of macrophages and other immune cells in the TME using flow cytometry (9). Using a similar strategy (Supplementary Fig. S3), we analyzed distinct populations of PD-$L1^{high}$ cells in the TME (Table 1). Although PD-L1 was expressed by multiple cell types, the dominant population of PD-$L1^{high}$ cells in CMT167 orthotopic tumors was alveolar macrophages. The non-macrophage PD-$L1^{high}$ cells were comprised of dendritic cells, endothelial cells, and $CD45^-$ $CD31^-$ cells that likely include fibroblasts.

Both CMT167 cells and immune cells must express PD-L1 for sensitivity to PD-L1 inhibition

To assess the specific contribution of PD-L1 expression by cancer cells, we depleted PD-L1 in CMT167 cells using shRNA (Supplementary Fig. S4A–B) and assessed response to PD-L1 antibody blockade *in vivo*. As shown in Fig. 2E, depleting PD-L1 partially reduced primary tumor growth compared to control cells in mice receiving isotype antibody (25.5 ± 8.3 mm^3 shCON vs 9.2 ± 2.3 mm^3 shPD-L1, $P = 0.06$). However, anti-PD-L1 antibody further inhibited growth of CMT shPD-L1 tumors (9.2 ± 2.3 mm^3 isotype vs 1.1 ± 0.6 mm^3 anti-PD-L1, $P < 0.01$).

To evaluate the role of PD-L1 in the TME, we implanted CMT167 cells into wild type C57BL/6 and PD-L1 KO mice. CMT167 tumor growth was inhibited in PD-L1 KO mice compared with WT mice (Fig. 2H: WT 16.85 ± 2.894 mm^3 vs PD-L1 KO 1.753 ± 1.252 mm^3, $P = 0.003$). Due to the strong inhibition (~90%) of tumor growth, we were unable to determine whether CMT167 orthotopic tumors grown in PD-L1 KO mice respond to PD-1/PD-L1 immunotherapy. Based on these data, we propose that targeting PD-L1 on both cancer cells and cells of the TME is critical for the antitumor effects of PD-L1 inhibition.

Sensitivity of CMT167 subcutaneous tumors to PD-1/PD-L1 inhibition

To determine the importance of the lung TME in mediating the response to PD-1/PD-L1 inhibition, CMT167 cells were implanted subcutaneously in wild-type C57BL/6 mice. Tumor-bearing mice were treated with anti-PD-1 monoclonal antibody, anti-PD-L1, or control IgG starting one week after tumor implantation. In contrast to our orthotopic model, PD-1/PD-L1 antibody blockade had a modest effect only on CMT167 subcutaneous tumor

growth compared to tumor-bearing mice treated with control IgG (Fig. 3A: IgG2a 1202 ± 203.5 mm^3 vs anti-PD-1 605.7 ± 179.4 mm^3, $P = 0.0412$; IgG2b 1592 ± 285.6 mm^3 vs anti-PD-L1 1125 ± 251.5 mm^3, $P = 0.2547$).

We sought to determine whether the differential response of CMT167 orthotopic tumors and subcutaneous tumors to PD-1/PD-L1 antibody blockade was associated with differences in T-cell responses. Flow cytometric analysis (Supplementary Fig. S5) demonstrated that $CD8^+$ T cells were more abundant in CMT167 subcutaneous tumors compared to CMT167 orthotopic tumor-bearing lungs (Fig. 3B), but there was no significant difference in $CD4^+$ T cells (Fig. 3C), leading to a decreased CD4:CD8 ratio in CMT167 subcutaneous tumors (Fig. 3D). Although there was a higher frequency of PD-1^+ $CD8^+$ T cells in CMT167 subcutaneous tumors (Fig. 3E), there were fewer PD-1^+ $CD4^+$ T cells compared to CMT167 orthotopic tumor-bearing lungs (Fig. 3F). In CMT167 subcutaneous tumors, 69.34 ± 2.48% of $CD4^+$ T cells expressed Foxp3 (Fig. 3G), compared to 11.38 ± 0.43% of $CD4^+$ T cells in CMT167 orthotopic tumors, indicating regulatory T cells (Tregs) are more abundant in subcutaneous tumors. Thus, tumors generated by the identical lung cancer cell line implanted in different anatomical sites led to different T-cell responses.

Next, we examined PD-L1 expression in CMT167 subcutaneous tumors. CMT167 cells were implanted into GFP-expressing transgenic C57BL/6 mice, and after 2 weeks, subcutaneous tumors were analyzed by flow cytometry. As with CMT167 orthotopic tumors, a subset of both cancer cells (GFP^-) and stromal cells (GFP^+) expressed PD-L1 (Fig. 3H). Compared to CMT167 orthotopic tumors, GFP^- PD-$L1^{high}$ cancer cells were more abundant in CMT167 subcutaneous tumors, but GFP^+ PD-$L1^{high}$ TME cells were less abundant (Fig. 3H). Similar to CMT167 orthotopic tumors, the dominant population of PD-$L1^{high}$ cells in CMT167 flank tumors consisted of macrophages (Table 1). However, all the PD-$L1^{high}$ macrophages within subcutaneous tumors are recruited from the bone marrow and circulation, and as expected, PD-$L1^{high}$ alveolar macrophages were not detected. There was a higher proportion of $CD11b^+Ly6G^+$PD-$L1^{high}$ cells in CMT167 subcutaneous tumors, which could represent either neutrophils or myeloid-derived suppressor cells (MDSCs).

Orthotopic lung tumors differ in sensitivity to anti-PD-1/PD-L1 therapy

We examined the response of a second K-Ras mutant murine cell line, LLC, in our orthotopic model. In contrast with CMT167 tumors, LLC orthotopic tumor growth was not inhibited by PD-1/PD-L1 antibody blockade (Fig. 4A and 4B). Immunofluorescent staining of LLC tumors for CD3ε (Fig. 4C) failed to show the dense nests of TILs found in CMT167 tumors, even in mice treated with PD-1/PD-L1 neutralizing antibodies. In cancer cells recovered from GFP-expressing transgenic mice, PD-L1 mRNA expression was lower in LLC cells (Fig. 2C–D), indicating that LLC cells express less PD-L1 than CMT167 cells *in vivo*. Increases in PD-L1 expression on cancer cells and in PD-$L1^{high}$ cells in the TME were less in LLC tumors than in CMT167 tumors (Fig. 4D–E).

CMT167 and LLC orthotopic tumors activate T lymphocytes to a similar extent

To determine whether the differential response of CMT167 and LLC orthotopic lung tumors to PD-1/PD-L1 inhibition was due to differences in T-cell activation, FFPE lung sections

from tumor-bearing animals were stained for $CD3^+$ cells and TILs were counted (Fig. 5A–B). Although there were more tumor-infiltrating $CD3^+$ T lymphocytes per high-power field in CMT167 tumors (Fig. 5C), abundant $CD3^+$ T lymphocytes were also detected within LLC tumors. Immunodepletion of $CD8^+$ T cells increased LLC tumor growth to a similar degree as CMT167 tumors (Fig. 5D), indicating that $CD8^+$ T cells constrain CMT167 and LLC tumors to a similar extent. Flow cytometric analysis of orthotopic tumor-bearing lungs demonstrated a decrease in $CD8^+$ T cells (as a percentage of $CD45^+$ cells) in LLC orthotopic tumors compared to uninjected lungs (Fig. 5E), but no difference in $CD4^+$ T cells (Fig. 5F). CD44 and CD69 expression on $CD8^+$ T cells was detected in both CMT167 and LLC orthotopic lung tumors (Supplementary Fig. S6B-C), suggesting T cells are activated by both tumors. Moreover, both CMT167 and LLC orthotopic lung tumors induced PD-1 expression on $CD8^+$ and $CD4^+$ T cells (Fig. 5G–H). Thus, in contrast with CMT167 subcutaneous tumors, the insensitivity of LLC tumors to anti-PD-1/PD-L1 was not associated with differences in PD-1 expression on T lymphocytes.

Induction of PD-L1 expression on macrophages in vitro is mediated by IL7 and IL15

We hypothesized that differences in PD-L1 expression on non-tumor cells in the lung were mediated by differences between the secretomes of CMT167 and LLC cells. To identify factors that up-regulate PD-L1 expression on macrophages, BMDMs were stimulated with conditioned media (CM) from each cell line. Addition of CM from either cell line increased PD-L1 expression at both the transcriptional and protein level (Fig. 6A–B). However, CMT167 CM increased PD-L1 expression more than LLC CM (Fig. 6A). Analysis of genes that code for secreted proteins expressed ≥ 5-fold higher in CMT167 compared to LLC cells *in vivo* revealed increases in IL7 and IL15 (Supplementary Fig. S7, Fig. 6C), which have been shown to induce PD-L1 expression on macrophages (16). *In vitro*, neutralization of both IL7 and IL15 with monoclonal antibodies blocked upregulation of PD-L1 on BMDMs induced by CMT167 CM, whereas neutralization of either IL7 or IL15 alone had no effect (Fig. 6D).

Discussion

NSCLC cells and immune cells in the TME can inhibit antitumor T cells through multiple pathways, including through coinhibitory receptors such as PD-1. Pharmacologic antibodies targeting PD-1 or its ligand PD-L1 can relieve inhibition of antitumor T cells, resulting in immune attack on tumors (2). These agents have shown efficacy in clinical trials for several types of cancer (17, 18), resulting in FDA approval for use of these agents for treatment of NSCLC and melanoma. However, response rates in NSCLC patients have ranged from 14.5% to 20% (3–7). Developing patient-selection criteria for these agents and rational combinations with other therapies requires a better understanding of factors that mediate response to immune checkpoint inhibitors. One critical issue is the contribution of the TME to anti-PD-1/PD-L1 therapy.

In this study, we have compared responses to anti-PD-1/PD-L1 therapy in several immunocompetent models of lung cancer. Our data support a system in which intrinsic properties of the cancer cells, as well as interactions between cancer cells and immune cells

in the TME, determine the response to PD-1/PD-L1 inhibitors. Whereas anti-PD-1/PD-L1 therapy inhibited CMT167 orthotopic lung tumors by 95%, CMT167 subcutaneous tumors were only inhibited by 30%. Silencing PD-L1 expression in CMT167 cells resulted in smaller orthotopic tumors that remained sensitive to anti-PD-L1 therapy, suggesting PD-L1 expression in the TME plays a role in immune escape of tumors. Moreover, CMT167 orthotopic tumors in PD-L1 KO mice are approximately $1/10^{th}$ the size of CMT167 orthotopic tumors in WT mice, which indicates that PD-L1 on non-tumor cells can limit antitumor immunity. Since the immunogenicity of CMT167 cells is identical in both orthotopic and subcutaneous models, we propose that specific features of the lung TME are critical for mediating the response to PD-1/PD-L1 inhibitors.

TILs have been investigated as a biomarker for response to anti-PD-1/PD-L1 therapy. The presence of TILs was associated with local PD-L1 expression in both primary and metastatic melanoma tumors (19). The presence of tumor $CD8^+$ T cells and PD-1 expression in patients may represent positive predictive biomarkers for anti-PD-1/PD-L1 therapy (20). A threshold level of intratumor $CD8^+$ PD-1 expression dictates therapeutic response to anti-PD-1 therapy (21). In our studies, PD-1 expression on $CD8^+$ T cells did not predict response to anti-PD-1/PD-L1 therapy, since the frequency of PD-1^+ $CD8^+$ T cells was higher in CMT167 subcutaneous tumors than CMT167 orthotopic tumors, and comparable between CMT167 orthotopic tumors and LLC orthotopic tumors. However, PD-1 can be induced in multiple contexts, including recently activated T cells and subsets of exhausted cells (22). Given this complexity and the evolving understanding of which cells confer the therapeutic benefit of PD-1/PD-L1 blockade (23–25), we have avoided describing the PD-1^+ T cells found in our studies as exhausted. However, we observed more Tregs in CMT167 subcutaneous tumors than in CMT167 orthotopic tumors, which may explain why subcutaneous tumors are less responsive to anti-PD-1/PD-L1 therapy. In our studies, there were also fewer PD-1^+ $CD4^+$ T cells in CMT167 subcutaneous tumors than in CMT167 orthotopic tumors. Several roles for $CD4^+$ T cells in antitumor immunity have been reported, including secretion of effector cytokines such as IFNγ (26, 27) and IL4 (28, 29), recruitment of effector cells including eosinophils and macrophages (30, 31), and provision of help to $CD8^+$ T cells for optimal priming and effector function (32, 33) and generation of $CD8^+$ memory T cells (34). Whether subsets of PD-1^+ T cells differ between CMT167 orthotopic tumors, LLC orthotopic tumors, and CMT167 subcutaneous tumors will be the subject of future studies.

In CMT167 orthotopic tumors, PD-L1 was upregulated on cancer cells and alveolar macrophages. However, in CMT167 subcutaneous tumors, PD-L1 was expressed mainly on cancer cells, macrophages recruited from the circulation, and $CD11b^+$ $Ly6G^+$ cells that may represent neutrophils or MDSCs. Since the populations of macrophages in subcutaneous tumors are different from those in lung tumors, we hypothesize PD-$L1^+$ alveolar macrophages have different functions than PD-$L1^+$ macrophages recruited from the circulation. However, proving that alveolar macrophages are responsible for differences between orthotopic tumors and subcutaneous tumors is challenging, because resident alveolar macrophages cannot be selectively depleted from the lungs. Conversely, alveolar macrophages injected into the flank would not be expected to maintain their phenotype in a different microenvironment. Effector cell populations responsible for killing tumor cells are also likely different between CMT167 orthotopic tumors and subcutaneous tumors, similar

to what was shown for antibody-mediated killing of melanoma cells grown in different anatomical sites (35). One challenge in comparing orthotopic tumors and subcutaneous tumors is that analysis of the lung TME includes regions of normal lung, whereas analysis of the subcutaneous TME is limited to tumor-infiltrating cells. Thus, comparison of the relative abundance of immune cell subpopulations in different tumor models is difficult.

A second lung cancer cell line (LLC) implanted into the same lung microenvironment as CMT167 cells is less sensitive to PD-1/PD-L1 inhibition, with less induction of PD-L1 expression on cells in the TME. Consistent with these data, CMT167 CM upregulated PD-L1 expression on BMDMs *in vitro* more than LLC CM, indicating soluble factors produced by cancer cells contribute to induction of PD-L1 in the TME. Analysis of genes that code for secreted proteins demonstrated that CMT167 cells express higher levels of IL7 and IL15, which have been shown to induce PD-L1 expression on macrophages (16). *In vitro*, neutralization of both IL7 and IL15 with monoclonal antibodies blocked upregulation of PD-L1 on BMDMs induced by CMT167 CM. Neutralization of either IL7 or IL15 alone had no effect, which suggests these cytokines synergize to induce PD-L1 expression on BMDMs. Future studies will explore this potential synergy, and whether blocking these factors may represent an approach to prevent T-cell exhaustion in lung cancer. The relative contribution of PD-L1 on cancer cells and cells in the TME to sensitivity to PD-1/PD-L1 inhibition also remains a subject for future investigation.

Since our data demonstrate that both CMT167 and LLC cell lines express oncogenic K-Ras, the differences in response to PD-L1/PD-1 inhibitors are not related to the oncogenic driver. The differential responses of CMT167 and LLC tumors to PD-L1 antibody blockade are also unlikely to be due to differences in the immunogenicity of the cancer cells, since activated T lymphocytes were detected within both tumors, and growth of orthotopic tumors formed by both cell lines was increased to the same extent by $CD8^+$ T-cell immunodepletion. Moreover, both CMT167 and LLC orthotopic tumors induce expression of CD44, CD69, and PD-1 on T cells. One difference is that CMT167 cells represent an epithelial cell line that expresses abundant E-cadherin, whereas LLC cells are mesenchymal and express little E-cadherin (Supplemental Fig S8). Mesenchymal NSCLC cell lines express higher levels of PD-L1 and are more responsive to anti-PD-L1 blockade (36). Our study demonstrates the reverse, with the more epithelial CMT167 cells expressing higher levels of PD-L1 *in vivo* and demonstrating greater response to PD-1/PD-L1 inhibition than the more mesenchymal LLC cells. However, CMT167 cells and LLC cells also differ in their cytokine profile, both *in vitro* and *in vivo*. Thus, the soluble factors produced by the cancer cell may be a better predictor of response to PD-1/PD-L1 inhibition than the state of differentiation. Although *JAK* mutations are a primary resistance mechanism to anti-PD-1 therapy in melanoma and colon cancer (37), genetic analysis of LLC cells revealed no mutations in either *JAK1* or *JAK2* (Supplemental Fig S8), and *JAK* mutations are therefore not the reason LLC tumors are insensitive to anti-PD-1/PD-L1 therapy.

In summary, we conclude that understanding basic mechanisms regulating immune checkpoints and testing rational combinations of checkpoint inhibitors require an orthotopic model, in which tumors develop in the appropriate microenvironment. The response to these agents will depend on the nature of the cancer cells, as well as interactions between cancer

cells and non-cancer cells present in the lung. Defining the factors that regulate PD-L1 expression on both cancer cells and cells of the TME will provide targets for the treatment of lung cancer.

Supplementary Material

Refer to Web version on PubMed Central for supplementary material.

Acknowledgments

Financial Support: This work was supported by the United States Department of Veterans Affairs Biomedical Laboratory Research and Development Service (Career Development Award IK2BX001282 to HYL), the NIH/NCI (R01 CA162226 and R01 CA108610 to RAN, and Colorado Lung SPORE P50 CA058187 to HYL and RAN), and the Cancer League of Colorado, Inc. (Research Grant to HYL). The Flow Cytometry and the Genomics and Microarray Shared Resources at the University of Colorado receive direct funding support from the NCI through the Cancer Center Support Grant P30CA046934.

The authors gratefully acknowledge use of the services and facilities of the Flow Cytometry and the Genomics and Microarray Shared Resources at the University of Colorado Cancer Center.

References

1. Jin HT, Ahmed R, Okazaki T. Role of PD-1 in regulating T-cell immunity. Current topics in microbiology and immunology. 2011; 350:17–37. [PubMed: 21061197]
2. Pardoll DM. The blockade of immune checkpoints in cancer immunotherapy. Nature reviews Cancer. 2012; 12(4):252–64. [PubMed: 22437870]
3. Borghaei H, Paz-Ares L, Horn L, Spigel DR, Steins M, Ready NE, et al. Nivolumab versus Docetaxel in Advanced Nonsquamous Non-Small-Cell Lung Cancer. The New England journal of medicine. 2015
4. Brahmer J, Reckamp KL, Baas P, Crino L, Eberhardt WE, Poddubskaya E, et al. Nivolumab versus Docetaxel in Advanced Squamous-Cell Non-Small-Cell Lung Cancer. The New England journal of medicine. 2015; 373(2):123–35. [PubMed: 26028407]
5. Gettinger SN, Horn L, Gandhi L, Spigel DR, Antonia SJ, Rizvi NA, et al. Overall Survival and Long-Term Safety of Nivolumab (Anti-Programmed Death 1 Antibody, BMS-936558, ONO-4538) in Patients With Previously Treated Advanced Non-Small-Cell Lung Cancer. Journal of clinical oncology : official journal of the American Society of Clinical Oncology. 2015; 33(18):2004–12. [PubMed: 25897158]
6. Rizvi NA, Mazieres J, Planchard D, Stinchcombe TE, Dy GK, Antonia SJ, et al. Activity and safety of nivolumab, an anti-PD-1 immune checkpoint inhibitor, for patients with advanced, refractory squamous non-small-cell lung cancer (CheckMate 063): a phase 2, single-arm trial. The Lancet Oncology. 2015; 16(3):257–65. [PubMed: 25704439]
7. Garon EB, Rizvi NA, Hui R, Leighl N, Balmanoukian AS, Eder JP, et al. Pembrolizumab for the treatment of non-small-cell lung cancer. The New England journal of medicine. 2015; 372(21): 2018–28. [PubMed: 25891174]
8. Poczobutt JM, Nguyen TT, Hanson D, Li H, Sippel TR, Weiser-Evans MC, et al. Deletion of 5-Lipoxygenase in the Tumor Microenvironment Promotes Lung Cancer Progression and Metastasis through Regulating T Cell Recruitment. Journal of immunology. 2015
9. Poczobutt JM, Gijon M, Amin J, Hanson D, Li H, Walker D, et al. Eicosanoid profiling in an orthotopic model of lung cancer progression by mass spectrometry demonstrates selective production of leukotrienes by inflammatory cells of the microenvironment. PLoS One. 2013; 8(11):e79633. [PubMed: 24244531]
10. Li H, Sorenson AL, Poczobutt J, Amin J, Joyal T, Sullivan T, et al. Activation of PPARgamma in myeloid cells promotes lung cancer progression and metastasis. PLoS One. 2011; 6(12):e28133. [PubMed: 22145026]

11. Weiser-Evans MC, Wang XQ, Amin J, Van Putten V, Choudhary R, Winn RA, et al. Depletion of cytosolic phospholipase A2 in bone marrow-derived macrophages protects against lung cancer progression and metastasis. Cancer Res. 2009; 69(5):1733–8. [PubMed: 19208832]
12. Layton MG, Franks LM. Heterogeneity in a spontaneous mouse lung carcinoma: selection and characterisation of stable metastatic variants. Br J Cancer. 1984; 49(4):415–21. [PubMed: 6324836]
13. Trapnell C, Pachter L, Salzberg SL. TopHat: discovering splice junctions with RNA-Seq. Bioinformatics. 2009; 25(9):1105–11. [PubMed: 19289445]
14. Trapnell C, Hendrickson DG, Sauvageau M, Goff L, Rinn JL, Pachter L. Differential analysis of gene regulation at transcript resolution with RNA-seq. Nature biotechnology. 2013; 31(1):46–53.
15. Justilien V, Regala RP, Tseng IC, Walsh MP, Batra J, Radisky ES, et al. Matrix metalloproteinase-10 is required for lung cancer stem cell maintenance, tumor initiation and metastatic potential. PLoS One. 2012; 7(4):e35040. [PubMed: 22545096]
16. Kinter AL, Godbout EJ, McNally JP, Sereti I, Roby GA, O'Shea MA, et al. The common gamma-chain cytokines IL-2, IL-7, IL-15, and IL-21 induce the expression of programmed death-1 and its ligands. Journal of immunology. 2008; 181(10):6738–46.
17. Brahmer JR, Tykodi SS, Chow LQ, Hwu WJ, Topalian SL, Hwu P, et al. Safety and activity of anti-PD-L1 antibody in patients with advanced cancer. The New England journal of medicine. 2012; 366(26):2455–65. [PubMed: 22658128]
18. Topalian SL, Hodi FS, Brahmer JR, Gettinger SN, Smith DC, McDermott DF, et al. Safety, activity, and immune correlates of anti-PD-1 antibody in cancer. The New England journal of medicine. 2012; 366(26):2443–54. [PubMed: 22658127]
19. Taube JM, Anders RA, Young GD, Xu H, Sharma R, McMiller TL, et al. Colocalization of inflammatory response with B7-h1 expression in human melanocytic lesions supports an adaptive resistance mechanism of immune escape. Sci Transl Med. 2012; 4(127):127ra37.
20. Tumeh PC, Harview CL, Yearley JH, Shintaku IP, Taylor EJ, Robert L, et al. PD-1 blockade induces responses by inhibiting adaptive immune resistance. Nature. 2014; 515(7528):568–71. [PubMed: 25428505]
21. Ngiow SF, Young A, Jacquelot N, Yamazaki T, Enot D, Zitvogel L, et al. A Threshold Level of Intratumor CD8+ T-cell PD1 Expression Dictates Therapeutic Response to Anti-PD1. Cancer Research. 2015; 75(18):3800–11. [PubMed: 26208901]
22. Wherry EJ, Kurachi M. Molecular and cellular insights into T cell exhaustion. Nature reviews Immunology. 2015; 15(8):486–99.
23. Im SJ, Hashimoto M, Gerner MY, Lee J, Kissick HT, Burger MC, et al. Defining CD8+ T cells that provide the proliferative burst after PD-1 therapy. Nature. 2016; 537(7620):417–21. [PubMed: 27501248]
24. Spitzer MH, Carmi Y, Reticker-Flynn NE, Kwek SS, Madhireddy D, Martins MM, et al. Systemic Immunity Is Required for Effective Cancer Immunotherapy. Cell. 2017; 168(3):487–502. e15. [PubMed: 28111070]
25. Huang AC, Postow MA, Orlowski RJ, Mick R, Bengsch B, Manne S, et al. T-cell invigoration to tumour burden ratio associated with anti-PD-1 response. Nature. 2017
26. Xie Y, Akpinarli A, Maris C, Hipkiss EL, Lane M, Kwon EK, et al. Naive tumor-specific CD4(+) T cells differentiated in vivo eradicate established melanoma. The Journal of experimental medicine. 2010; 207(3):651–67. [PubMed: 20156973]
27. Quezada SA, Simpson TR, Peggs KS, Merghoub T, Vider J, Fan X, et al. Tumor-reactive CD4(+) T cells develop cytotoxic activity and eradicate large established melanoma after transfer into lymphopenic hosts. The Journal of experimental medicine. 2010; 207(3):637–50. [PubMed: 20156971]
28. Tepper RI, Coffman RL, Leder P. An eosinophil-dependent mechanism for the antitumor effect of interleukin-4. Science. 1992; 257(5069):548–51. [PubMed: 1636093]
29. Nishimura T, Iwakabe K, Sekimoto M, Ohmi Y, Yahata T, Nakui M, et al. Distinct role of antigen-specific T helper type 1 (Th1) and Th2 cells in tumor eradication in vivo. The Journal of experimental medicine. 1999; 190(5):617–27. [PubMed: 10477547]

30. Hung K, Hayashi R, Lafond-Walker A, Lowenstein C, Pardoll D, Levitsky H. The central role of CD4(+) T cells in the antitumor immune response. The Journal of experimental medicine. 1998; 188(12):2357–68. [PubMed: 9858522]

31. Corthay A, Skovseth DK, Lundin KU, Rosjo E, Omholt H, Hofgaard PO, et al. Primary antitumor immune response mediated by CD4+ T cells. Immunity. 2005; 22(3):371–83. [PubMed: 15780993]

32. Schietinger A, Philip M, Liu RB, Schreiber K, Schreiber H. Bystander killing of cancer requires the cooperation of CD4(+) and CD8(+) T cells during the effector phase. The Journal of experimental medicine. 2010; 207(11):2469–77. [PubMed: 20921286]

33. Tran E, Turcotte S, Gros A, Robbins PF, Lu YC, Dudley ME, et al. Cancer immunotherapy based on mutation-specific CD4+ T cells in a patient with epithelial cancer. Science. 2014; 344(6184): 641–5. [PubMed: 24812403]

34. Shedlock DJ, Shen H. Requirement for CD4 T cell help in generating functional CD8 T cell memory. Science. 2003; 300(5617):337–9. [PubMed: 12690201]

35. Lehmann B, Biburger M, Bruckner C, Ipsen-Escobedo A, Gordan S, Lehmann C, et al. Tumor location determines tissue-specific recruitment of tumor-associated macrophages and antibody-dependent immunotherapy response. Science Immunology. 2017; 2(7)

36. Chen L, Gibbons DL, Goswami S, Cortez MA, Ahn YH, Byers LA, et al. Metastasis is regulated via microRNA-200/ZEB1 axis control of tumour cell PD-L1 expression and intratumoral immunosuppression. Nat Commun. 2014; 5:5241. [PubMed: 25348003]

37. Shin DS, Zaretsky JM, Escuin-Ordinas H, Garcia-Diaz A, Hu-Lieskovan S, Kalbasi A, et al. Primary Resistance to PD-1 Blockade Mediated by JAK1/2 Mutations. Cancer Discov. 2017; 7(2): 188–201. [PubMed: 27903500]

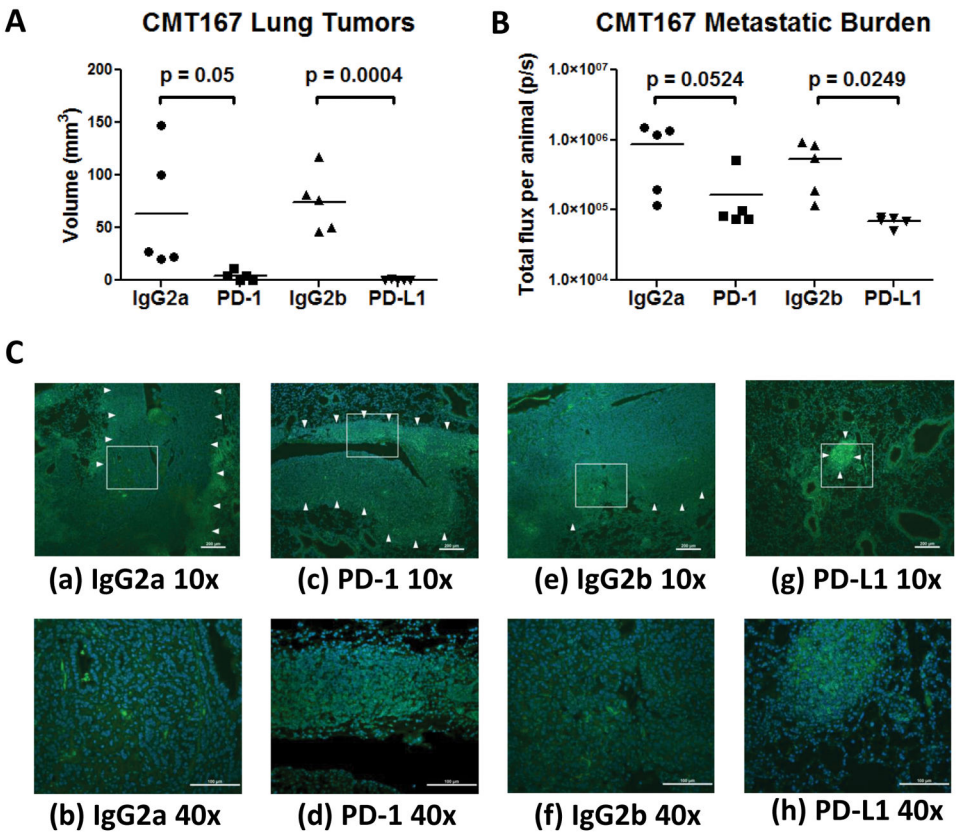

Fig. 1.

PD-1 and PD-L1 antibody blockade inhibit growth of CMT167 orthotopic lung tumors. CMT167 orthotopic tumor-bearing mice were injected with anti-PD-1, anti-PD-L1, or isotype control antibody ($n = 5$ for each group). Effects of anti-PD-1/anti-PD-L1 therapy on (A) CMT167 primary tumor volume and (B) metastatic burden in the other lung lobes. Each point represents an individual mouse. (C) Representative CD3 immunostaining (FITC, green) of sections from mice treated with control IgG2a (a and b), anti-PD-1 (c and d), control IgG2b (e and f), and anti-PD-L1 (g and h). Nuclei were stained with DAPI (blue); tumor borders are indicated by arrowheads. (a,c,e,g) Low power image (10x), scale bar = 200 μm; (b,d,f,h) high power detail of boxed regions from low power images (40x), scale bar = 100 μm.

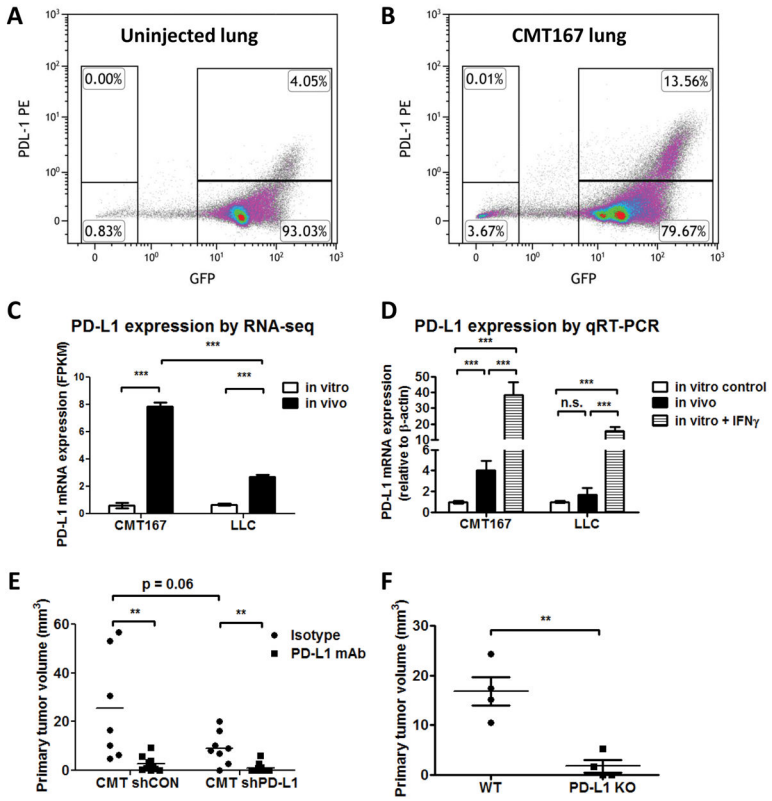

Fig. 2.

PD-L1 expression is upregulated on both cancer cells and in the TME in CMT167 orthotopic lung tumors. Representative flow cytometric plot from uninjected mice (A) and CMT167 tumor-bearing mice (B). Similar results were obtained in 5 independent experiments, with 2 mice in each pool. (C) PD-L1 mRNA expression from cancer cells recovered from tumor-bearing mice was analyzed by RNA-seq and compared to cancer cells in culture. Each RNA isolation represents a pool of 4–5 mice. (D) PD-L1 mRNA expression from cancer cells recovered from tumor-bearing mice was determined by qRT-PCR and compared with cells cultured *in vitro*, either in the presence or absence of IFNγ (3 separate RNA isolations). (E) Effects of depleting PD-L1 in CMT167 cells on primary tumor size. CMT shCON isotype $n = 7$, CMT shCON PD-L1 mAb $n = 8$, CMT shPD-L1 isotype $n = 10$, CMT shPD-L1 PD-L1 mAb $n = 10$. (F) CMT167 cells were implanted in the left lungs of wild-type C57BL/6 mice and PD-L1 KO mice ($n = 4$ for each group). Statistically significant differences are indicated as determined by one-way ANOVA (C–E) or Student unpaired *t* test (F), ** = $P < 0.01$, *** = $P < 0.001$.

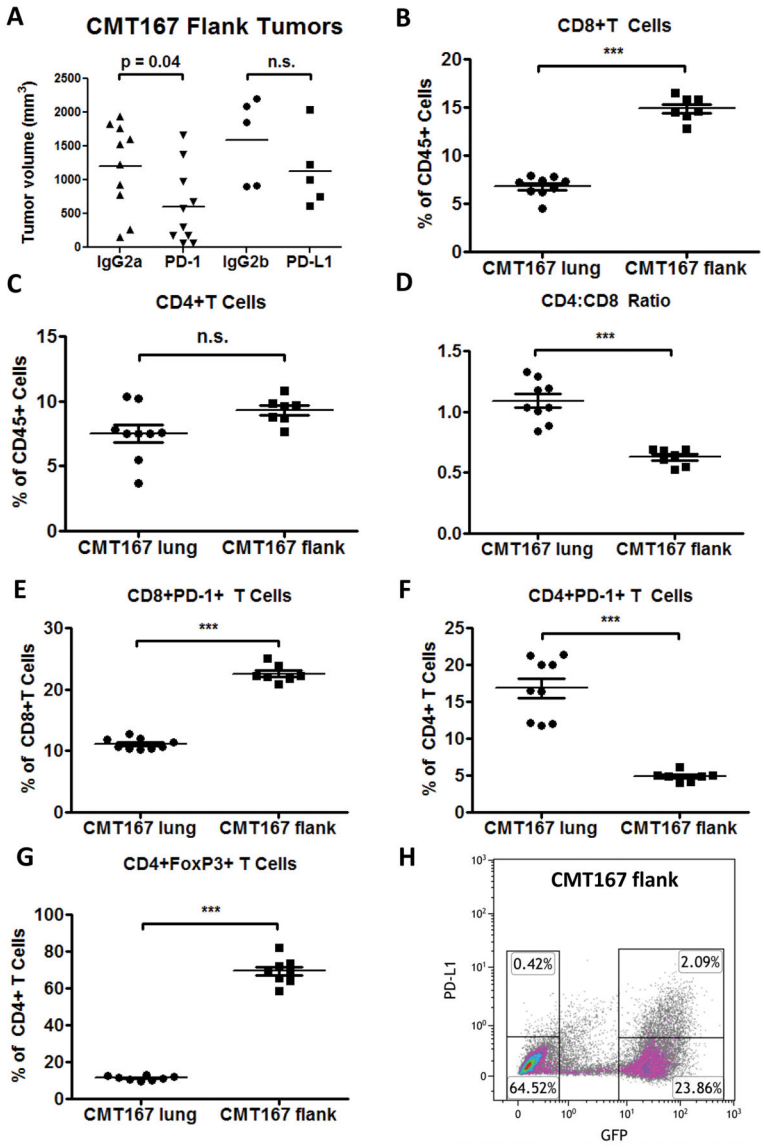

Fig. 3.

CMT167 subcutaneous tumors induce a T-cell response that is skewed toward CD8+ T cells and are less sensitive than CMT167 orthotopic tumors to anti-PD-1/PD-L1 therapy. (A) CMT167 subcutaneous tumor-bearing mice were injected with anti-PD-1, anti-PD-L1, or isotype control antibody ($n = 10$ for IgG2a and anti-PD-1 groups, $n = 5$ for IgG2b and anti-PD-L1 groups). CMT167 orthotopic tumor-bearing lungs ($n = 9$) and CMT167 subcutaneous tumors ($n = 7$) were analyzed by flow cytometry for (B) $CD8^+$ T cells, (C) $CD4^+$ T cells, (D) CD4:CD8 ratio, (E) PD-1 expression on $CD8^+$ T cells, (F) PD-1 expression on $CD4^+$ T cells, and (G) Foxp3 expression in $CD4^+$ T cells. Statistically significant differences are indicated as determined by Student unpaired *t* test; ** = $P < 0.01$, *** = $P < 0.001$. (H) PD-L1 expression was analyzed by flow cytometry in CMT167 subcutaneous tumors. Similar results were obtained in five independent mice.

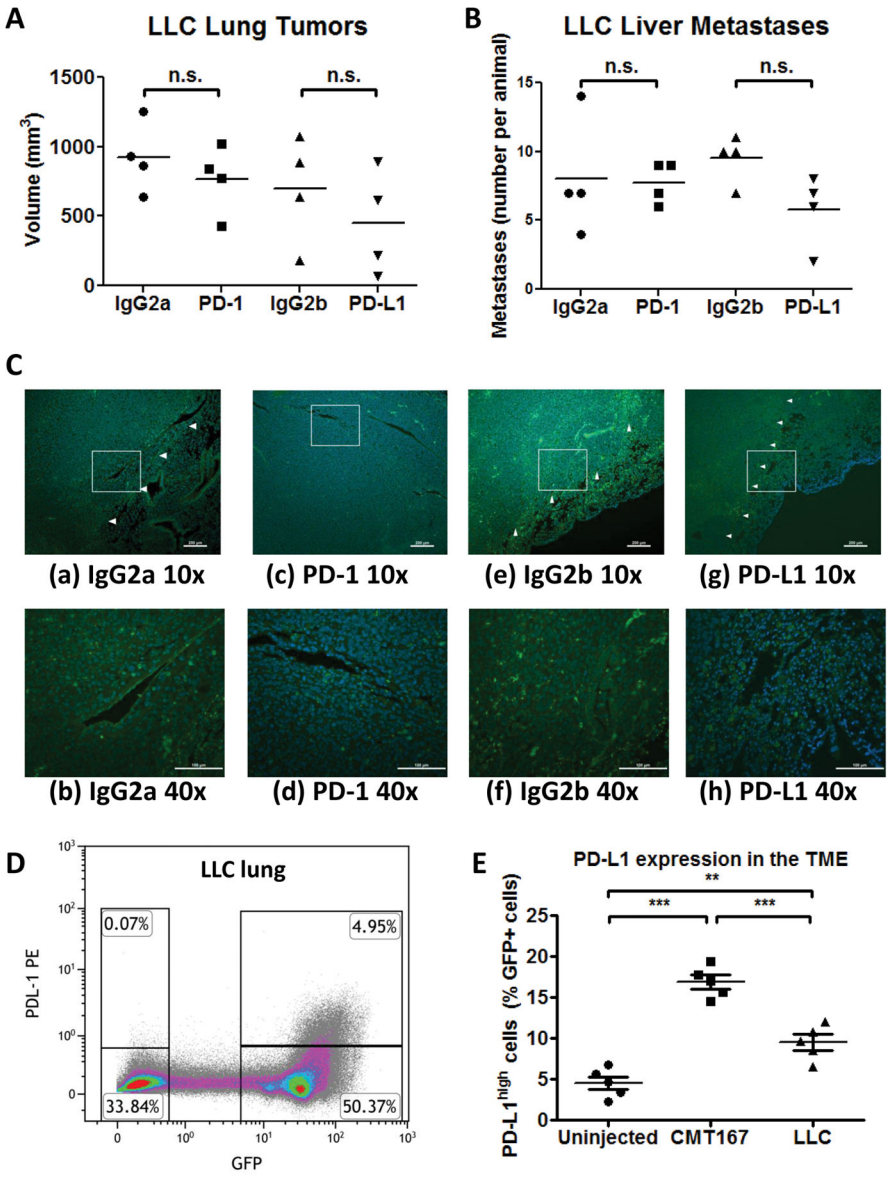

Fig. 4.

LLC orthotopic tumors are less sensitive than CMT167 orthotopic tumors to anti-PD-1/PD-L1 therapy. LLC orthotopic tumor-bearing mice were injected with anti-PD-1, anti-PD-L1, or isotype control antibody ($n = 4$ for each group). Effects of anti-PD-1/anti-PD-L1 therapy on (A) LLC primary tumor volume and (B) number of liver metastases. (C) Representative CD3 immunostaining of tissue sections from mice treated with control IgG2a (a and b), anti-PD-1 (c and d), control IgG2b (e and f), and anti-PD-L1 (g and h). Nuclei were stained with DAPI (blue); tumor borders are indicated by arrowheads. (a, c, e, g) Low power image (10x), scale bar = 200 μm; (b, d, f, h) high power detail of boxed regions from low power images (40x), scale bar = 100 μm. (D) Representative flow cytometric plot from LLC tumor-bearing mice. Similar results were obtained in 5 independent experiments consisting of 2 mice each. (E) The percentage of $GFP^{+}PD\text{-}L1^{high}$ cells in mice implanted with CMT167

tumors or LLC tumors was compared to uninjected mice. Each point represents an individual animal ($n = 5$ for each group). ** = $P < 0.01$, *** = $P < 0.001$.

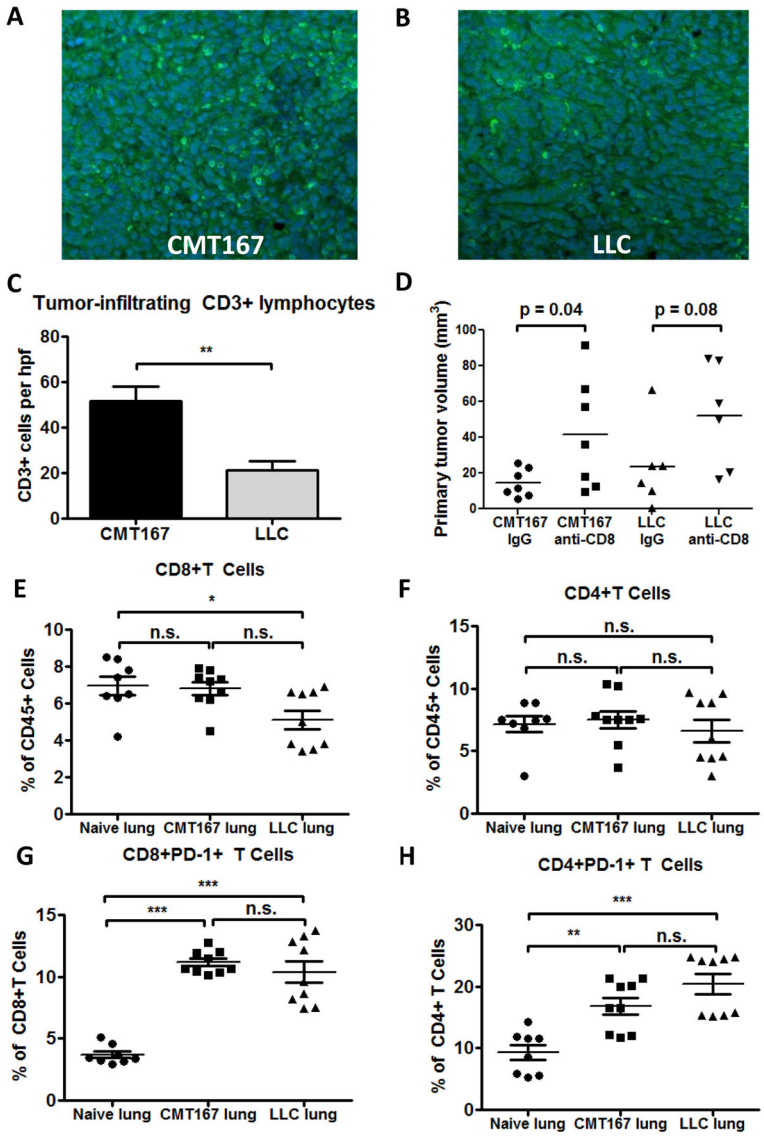

Fig. 5.

Both CMT167 orthotopic lung tumors and LLC orthotopic lung tumors generate an adaptive immune response and induce PD-1 expression on T cells. Tissue sections from CMT167 (representative image shown in Fig. 5A) and LLC (representative image shown in Fig. 5B) tumor-bearing mice were stained for CD3 (FITC, green) and nuclei were stained with DAPI (blue). Magnification x20. (C) Quantification of tumor-infiltrating lymphocytes in CMT167 tumors ($n = 9$) and LLC tumors ($n = 6$). (D) Effects of $CD8^+$ T cell immunodepletion on growth of CMT167 ($n = 7$ each group) and LLC orthotopic tumors ($n = 6$ each group). CMT167 ($n = 9$, same mice as in Fig. 3B–F) or LLC tumor-bearing lungs ($n = 9$) were analyzed by flow cytometry and compared with lungs from naive mice ($n = 8$) for (E) $CD8^+$ T cells, (F) $CD4^+$ T cells, (G) PD-1 expression on $CD8^+$ T cells, and (H) PD-1 expression on $CD4^+$ T cells. Statistically significant differences are indicated as determined by Student unpaired *t* test (C-D) or by one-way ANOVA (E-H); * = $P < 0.05$, ** = $P < 0.01$, *** = $P < 0.001$.

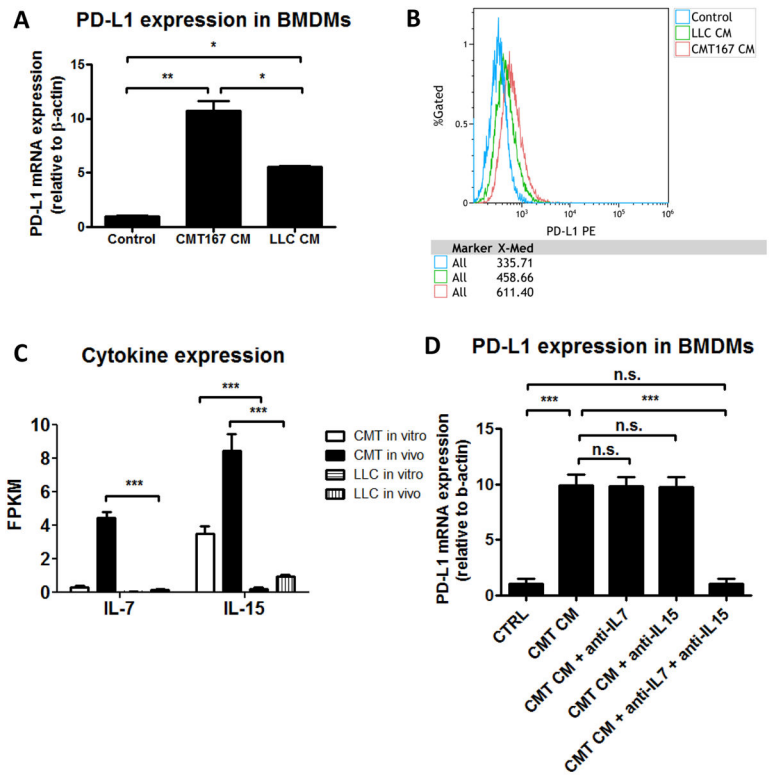

Fig. 6.

Conditioned media (CM) from CMT167 cells induces higher levels of PD-L1 in bone marrow derived macrophages than CM from LLC cells. (A) Bone marrow derived macrophages were treated with CM from CMT167 cells or LLC cells. Data represent the mean of 3 experiments using 3 separate isolations of CM. (B) A representative overlay of PD-L1 expression is shown from untreated BMDMs (blue), BMDMs treated with LLC CM (green), and BMDMs treated with CMT167 CM (red). Similar results were obtained in 3 independent experiments using 3 separate isolations of CM. (C) IL7 and IL15 mRNA expression was determined by RNA-seq from CMT167 cells and LLC cells, both *in vitro* and *in vivo*. (D) Effects of IL7 and IL15 neutralization on upregulation of PD-L1 on BMDMs induced by CMT167 CM. Data represent the mean and SEM from 3 independent experiments. Statistically significant differences are indicated as determined by one-way ANOVA; * = $P < 0.05$, ** = $P < 0.01$, *** = $P < 0.001$.

Table 1

Subsets of PD-L1^{high} cells in CMT167 and LLC tumors.

Cells (% of GFP+PD-L1^{high} by flow cytometry)	CMT167 orthotopic (n = 4 pools of 2 mice)	CMT167 subcutaneous (n = 7 tumors)	LLC orthotopic (n = 4 pools of 2 mice)
Alveolar macrophages	59.4 ± 4.98	N.D.	46.3 ± 4.40
Interstitial and monocyte-derived recruited macrophages	24.2 ± 2.03	**67.66 ± 2.29**	**45.6 ± 4.33**
Dendritic cells	4.0 ± 1.46	1.8 ± 1.60	1.5 ± 1.43
CD11b+Ly6G+ myeloid cells	N.D.	**28.66 ± 1.60**	2.5 ± 1.37
Endothelial cells	4.1 ± 1.44	1.8 ± 1.29	0.7 ± 0.66
Total PD-L1^{high} (% of GFP+ cells)	16.88 ± 0.84	**8.05 ± 1.90**	**9.53 ± 0.95**

Statistically significant differences by ANOVA compared to CMT167 orthotopic tumors are shown in bold. N.D. = not detected